Indian J Phys
DOI 10.1007/s12648-015-0830-5

ORIGINAL PAPER

Electronic structure, mechanical, and optical properties of $CaO{\cdot}Al_2O_3$ system: a first principles approach

A Hussain[1,2]*, S Mehmood[2], M N Rasool[2], S Aryal[1,3], P Rulis[1] and W Y Ching[1]

[1]Department of Physics and Astronomy, University of Missouri-Kansas City, Kansas City, MO 64110, USA

[2]Department of Physics, The Islamia University of Bahawalpur, Bahawalpur, Punjab 63100, Pakistan

[3]Department of Mathematics and Physics, Tennessee State University, Nashville, TN 37209, USA

Received: 29 October 2015 / Accepted: 07 December 2015

Abstract: A comprehensive study of the structure, bonding, mechanical and optical properties of five stable phases within the calcium aluminate (Ca–Al–O) series with different CaO to Al_2O_3 proportions has been carried out using the density functional theory based orthogonalized linear combination of atomic orbitals (OLCAO) method. The phases are C3A, C12A7-crystal, CA, CA2, and CA6 and the oxygen deficient C12A7-electride phase. These five stable phases are wide band gap insulators with energy gap values ranging from 3.85 to 4.62 eV. The charge neutral C12A7-crystal has localized defective states in the gap whereas the C12A7-electride phase has a region of metallic bands of about 2 eV wide in the gap. Effective charge and bond order calculations reveal intimate details of electronic structure and bonding in relation to the aluminate contents in the series. It is shown that Al–O bonds dominate the Ca–O bonds in determining the crystal strength with CA6 having the highest and C12A7 having the lowest bond order density. Calculations of elastic coefficients and mechanical properties in these crystals show a high degree of diversity and anisotropic behavior consistent with the bond order calculations. The refractive index values from optical properties calculations are in good agreement with available literature. Other results furnish more insights for the Ca–Al–O series and provide the opportunity for further investigations on similar or more complicated quaternary systems with potential novel properties.

Keywords: Calcium alumina oxide; Electronic structure; Mechanical properties; Optical properties; Ab initio calculations

PACS Nos.: 62.20.-x; 71.15.Mb; 77.22.-d; 78.20.Ci

1. Introduction

Calcium aluminate cements (CACs) or calcium alumina oxides (Ca–Al–O) have superior refractory properties which make them important for various industrial applications such as floor forming and screeds, chemical resistant mortars and concretes, sewer applications, tile adhesives and protective laminations [1–3]. This class of ceramics is conventionally represented by the notation $nCaO{\cdot}mAl_2O_3$ (CnAm) for simplicity, because they are usually composed of main group metal oxides i.e. CaO and Al_2O_3. Calcium aluminates are synthesized through the heating of calcium oxide and aluminum oxide at higher temperatures. These laboratory calcium aluminates have a rich phase diagram (Fig. 1) that includes five stable compounds: (1) tricalcium aluminate/$3CaO{\cdot}Al_2O_3$ (C3A), (2) dodecacalcium hepta-aluminate/$12CaO{\cdot}7Al_2O_3$ (C12A7), (3) monocalcium aluminate/$CaO{\cdot}Al_2O_3$ (CA), (4) monocalcium dialuminate/$CaO{\cdot}2Al_2O_3$ (CA2), and (5) monocalcium hexa-aluminate/$CaO{\cdot}6Al_2O_3$ (CA6) [4]. Among these, the C12A7 phase has the lowest melting temperature (1722 °C) and CA6 has the highest (2156 °C) melting temperature [5].

Tricalcium aluminate (C3A) is the third most abundant component of ordinary Portland cement and has been extensively studied in the past. During this decade, a number of theoretical and experimental findings on C3A have been conducted, including the calculations of its electronic structure [6]. In another study, its elastic moduli

*Corresponding author, E-mail: altafiub@yahoo.com

Published online: 14 January 2016

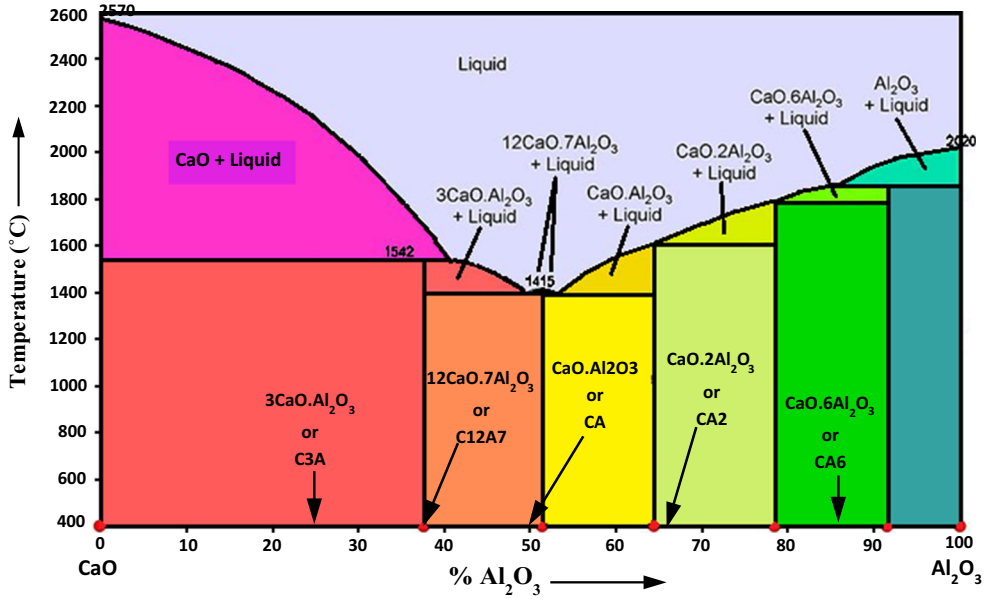

Fig. 1 (*Color online*) Phase diagram of calcium aluminate system

tensor along with the bulk mechanical properties have been calculated [7]. The calculated Young's modulus result ($E = 138.7$ GPa) has been found to be in good agreement with the value obtained from nano-indentation investigations performed by Velez [8]. More recently, Moon [9] has calculated the band structure and elastic properties of C3A by using high-pressure X-ray technique as well as first principles calculations.

In the recent past, C12A7 has emerged as a novel functional material with potential applications (e.g. as a catalyst) especially in electronic industry [10–12]. This crystal has a three dimensional framework structure that may contain extra-framework species such as O^{2-} [13, 14] and partially occupy cavities in the framework. Therefore, strictly speaking, it may not be considered as a perfect crystal in the conventional fashion because it does not have perfect long range order. However, Akola et al. [15] have reported that the calcium aluminate system has a glassy nature with a structural model comparable to C12A7. A sub-phase of C12A7, called the electride phase does not contain extra-framework species [16].

The CA phase bears similar proportions of CaO and Al_2O_3. It does not exist independently in nature but rather as a solid solution with C3A in CAC. CA2 and CA6 are alumina rich phases similar to CA. CA2 has a very low coefficient of thermal expansion (CTE) (i.e. 1.2×10^6 K^{-1} up to 372 K) and has been used as a thermal-shock-resistant refractory material [17]. CA6 is known as an interface phase in fiber-reinforced ceramic-oxide composites that facilitates the fiber pull-out and enhances the strength of the materials [18].

It has been observed that the existing experimental and theoretical findings on the various calcium aluminate phases appear to be scattered and are lacking a cohesive picture [6–18]. A comprehensive and fundamental study covering all stable phases and several properties would provide a unifying starting point for other research. In this article, we present the results of such a comprehensive study of five stoichiometric calcium aluminates: C3A ($x = 0.25$), C12A7 ($x = 0.368$, C12A7-crystal), CA ($x = 0.50$), CA2 ($x = 0.667$), and CA6 ($x = 0.857$) and the non-stoichiometric oxygen deficient electride phase of C12A7 (C12A7-electride). In all calculations we have used the density functional theory (DFT)-based orthogonalized linear combination of atomic orbitals (OLCAO) method [19] with the crystal structures first optimized using the Vienna ab initio simulation package (VASP) [20, 21]. The combination of these two methods is well suited for large complex systems and its successful application on many material systems has been fully acknowledged [22–25].

2. Crystal structures

The cubic form of C3A, as shown in Fig. 2(a), with four-fold coordinated Al was explored first by Burdick [26] and then by Mondal and Jeffery [27]. Single-crystal X-ray diffraction determined the atomic coordinates and lattice parameters [27, 28]. The structure contains sixfold rings centered on threefold axes and composed of two types of distorted AlO_4 tetrahedra. The holes inside and between the rings contain the Ca atoms. There are 80 such possible

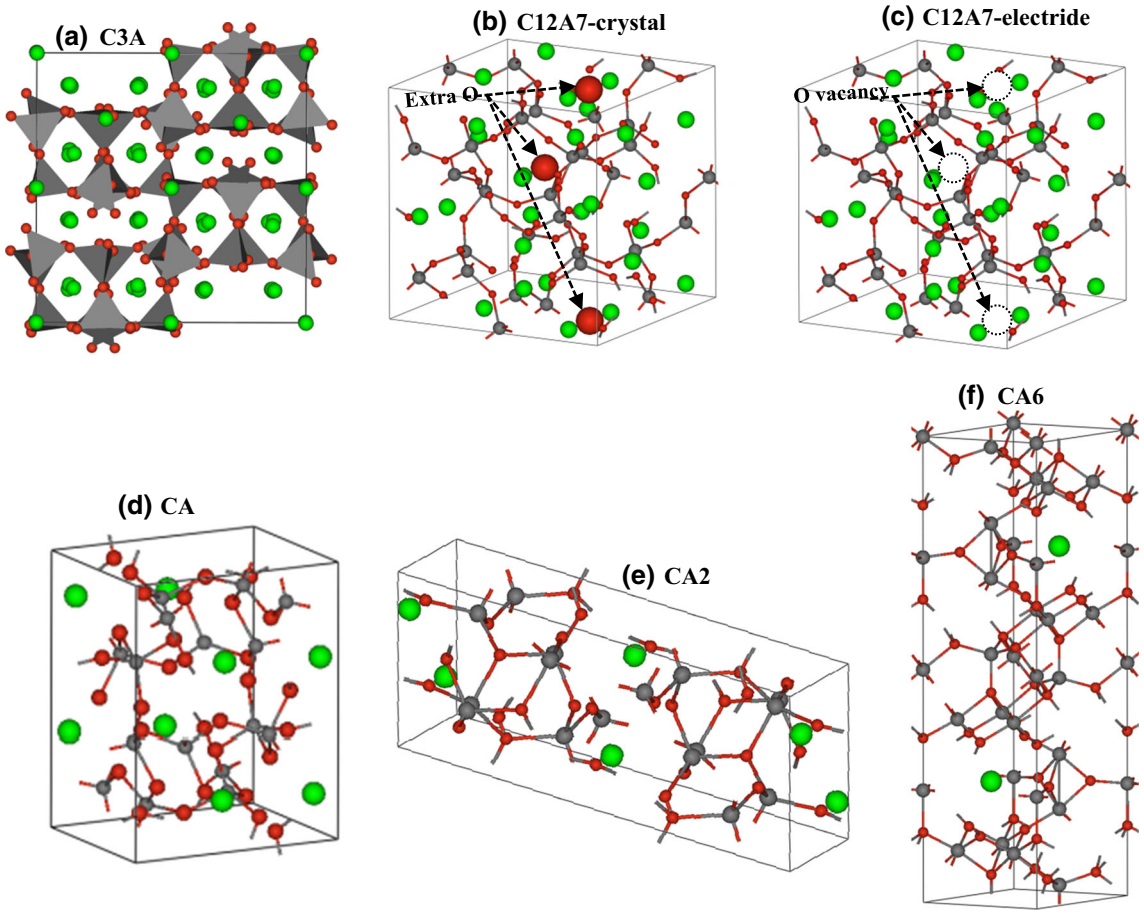

Fig. 2 (*Color online*) Crystal structures of various calcium aluminate phases: (**a**) Optimized crystal structure of C3A (*rosy brown* polyhedra represent AlO_4 tetrahedra), (**b**) C12A7-crystal, (**c**) C12A7-electride, (**d**) CA, (**e**) CA2, and (**f**) CA6. Al, *rosy brown*; Ca, *blue*; O, *green*

holes present in the unit cell, 72 of them are filled with Ca atoms leaving eight vacant holes on threefold axes at [1/8, 1/8, 1/8]. These structural holes facilitate the interaction with water molecules during the hydration process. There are eight separate Al_6O_{18} rings surrounding each of the eight vacant sites located around the corners of the sub-cells ($a' = a/2$). The six AlO_4 tetrahedra in the Al_6O_{18} ring are tilted alternately to each side of the ring. C3A represents the most complex crystal structure among all the phases discussed in this article.

The stoichiometric C12A7 phase has a cubic zeolite-like structure which is iso-structural with the mineral mayenite [Fig. 2(b)] [29]. The unit cell can be represented using the formula $[Ca_{24}Al_{28}O_{64}]^{4+}{\cdot}(O^{2-})_2$ or $(C12A7{:}O^{2-})$ and $[Ca_{24}Al_{28}O_{64}]^{4+}{\cdot}(e^-)_4$ or $(C12A7{:}e^-)$ for the electride phase. Here $[Ca_{24}Al_{28}O_{64}]^{4+}$ designates a three dimensional lattice framework containing 12 sub-nanometer cages per unit cell and the two O^{2-} ions are the extra-framework species occupying some of the framework cages [14, 15]. Al has relatively regular tetrahedral coordination partially linked by corner O atoms and bridging Ca atoms to form eight-membered AlO_4 rings. Ca atoms are sevenfold coordinated with four shorter bonds of 2.35 (2) and 2.39 (2) Å, two "long" bonds (2.59 Å), and an extra-long bond of 2.78 Å [30]. Figure 2(c) for the electride phase is the same as Fig. 2(b) with the only difference being the absence of the two extra-framework O [enlarged red circles in Fig. 2(b)].

CA has a low symmetry tridymite-like structure with six-membered rings of AlO_4 tetrahedra [Fig. 2(d)] [31]. Ca atoms occupy sites within the fully polymerized AlO_4 network. There are three Ca sites, two with Ca in octahedral coordination and a third one bonded to nine O atoms. The AlO_4 tetrahedra are found to be fully interconnected with equal proportions of CaO and Al_2O_3. Both CA and C3A have the largest number of non-equivalent sites in the crystals (Table 1).

The structure of CA2 has a long history of controversy which we briefly summarize to fully clarify the structure which we have used in this work. Its presence is initially reported in two independent investigations during 1937 [32, 33]. Goldsmith [34], Goria and Burdese [35] have

Table 1 Crystal structure data used in present study

	C3A	C12A7-crystal	C12A7-electride	CA	CA2	CA6
x (%age of Al_2O_3 content)	0.25	0.37	0.37	0.50	0.67	0.86
Crystal type	Cubic	Cubic	Cubic	Monoclinic	Monoclinic	Hexagonal
Space group (no.)	Pa3 (205)	I $\bar{4}$ 3d (220)	I $\bar{4}$ 3d (220)	$P2_1/c$ (14)	C2/c (15)	$P6_3/mmc$ (194)
Lattice parameters						
a (Å)	15.391	12.001	12.090	8.012	12.963	5.609
b (Å)	15.391	12.105	12.104	8.693	8.958	5.609
c (Å)	15.391	12.105	12.100	10.376	5.492	22.125
α	90.000°	89.998°	89.998°	90.000°	90.000°	90.00°
β	90.000°	89.998°	90.000°	95.044°	106.307°	90.00°
γ	90.000°	90.000°	90.000°	90.000°	90.000°	120.00°
Atoms/unit cell	264	118	116	56	48	64
Formula units/unit cell	24	2	2	8	4	2
Atom types (no. of atoms of different type)						
Ca	6 (4, 4, 8, 8, 24, 24)	1 (24)	1 (24)	2 (4 each)	1 (4)	1 (2)
Al	2 (24 each)	3 (16, 4, 8)	3 (16, 4, 8)	4 (4 each)	2 (8, 8)	5 (2, 2, 4, 4, 12)
O	6 (24 each)	3 (48, 16, 2)	2 (48, 16)	8 (4 each)	4 (4, 8, 8, 8)	5 (4, 4, 6, 12, 12)
Non-equivalent sites	14	7	6	14	7	11
scf *k*-points	4	14	14	35	84	60
OLCAO *k*-points	11	108	108	238	583	395

reported CA2 as monoclinic according to their X-ray diffraction results, but Goldsmith's optical measurements reveale that it can be either a hexagonal or a tetragonal phase. Filonenko and Laurov [36], on the other hand, have described that CA2 crystallizes in a tetragonal form. Later on, Boyko and Wisnyi [37] have suggested that CA2 forms a monoclinic crystal with a space group C2/*c*; Cockayne and Robertson [38] have concluded that this phase is complex hexagonal. However, Goodwin and Lindop [39] have confirmed the monoclinic structure [Fig. 2(e)], which is now the accepted structure for CA2 and the same is considered in this study. Ca atom and one of the O atoms, i.e. O1, lie in special positions with the Ca ions along the crystallographic *b* axis. Each Ca has seven nearest neighbor (NN) O ions of varying separations between 2.33 and 2.88 Å. The Al sites are each at the center of almost regular AlO_4 tetrahedra.

CA6 [Fig. 2(f)] is known as a stable hexagonal phase which exists at the interface of fiber-reinforced ceramic-oxide composites [18]. Its crystal structure has been reported by Kato and Saalfeld. Later Utsunomiya [40] has determined that it is iso-structural with the mineral magneto-plumbite. In this phase, Al atoms are distributed over three octahedral sites, one tetrahedral site and one trigonal–bipyramidal site.

Finally, the summarized crystal structure data are provided in Table 1 along with the number of *k*-points which have been used in the OLCAO calculations to be described below. It has been observed that all structures are large and complex with low symmetry and with many nonequivalent sites within the unit cell containing a combination of Ca–O and Al–O bonds.

3. Method of calculations

In order to calculate the electronic structure, inter-atomic bonding, and optical properties we employed the first-principles based OLCAO method [19]. The OLCAO method was based on the local density approximation (LDA) of DFT [41, 42]. This approach was considered as both accurate and efficient when dealing with complex crystalline [23, 25, 43, 44] and non-crystalline [22, 45] materials. In OLCAO, the solid state wave function was expanded in terms of atomic orbitals which were themselves expanded as Gaussian type orbitals (GTOs). Three types of basis sets were used for different properties: the full basis (FB), which consists of the core orbitals, occupied valence orbitals and the next empty shell of unoccupied orbitals used for the determination of the self-

consistent field (SCF) potential, band structures and density of states (DOS). For Ca–Al–O system, the FB consists of Ca- (1*s*, 2*s*, 2*p*, 3*s*, 3*p*, 3*d*, 4*s*, 4*p*, 4*d*, and 5*s*), Al- (1*s*, 2*s*, 2*p*, 3*s*, 3*p*, and 3*d*), and O-(1*s*, 2*s*, 2*p*, 3*s*, and 3*p*). For optical properties calculations, an extended basis (EB) set was used, which includes one additional shell of empty orbitals to further improve the accuracy of the higher states in the conduction band (CB). On the other hand, for effective charge (Q^*) and bond order (BO) calculations using the Mulliken analysis [46], a minimal basis (MB) set was used which provides a more localized basis for such analysis. The crystal potential achieved self-consistency when the total energy converged to 0.0001 a.u. (Hartree atomic units). A sufficient number of *k*-points for SCF iterations and DOS optical spectra evaluations were used depending on crystal size (see Table 1). Additional tests with more *k*-points showed no discernible differences with respect to energy convergence and other computed properties (e.g. density of states, bond order, etc.). For consistency, all crystal structures were first optimized using the VASP package [20, 21]. The versatility of using different basis sizes for different purposes is instrumental in enabling OLCAO to have high efficiency and accuracy in the calculations of a variety of properties.

One of the most useful features of the OLCAO method is the quantitative evaluation of the effective charge Q^* on each atom and the BO values for each pair of atoms in the crystal without any assumption on atomic size or radius. Q^*_α provides information about charge transfer (gain or loss) from each neutral atom α in terms of the valence electrons according to:

$$Q^*_\alpha = \sum_i \sum_{n,occ} \sum_{j,\beta} C^{*n}_{i\alpha} C^n_{j\beta} S_{i\alpha,j\beta} \tag{1}$$

where $C^n_{j\beta}$ are the eigenvector coefficients, n is the band index, j and β label the orbital and atom in the crystal and $S_{i\alpha,j\beta}$ are overlap integrals. BO (also called the overlap population) is a measure of the relative strength of a bond between a pair of atoms and is the microscopic origin for the mechanical properties of materials. For atomic pairs of the same type the BO values generally scale with the bond length, but they can also be influenced by the near-by atoms and the local geometric environment. This is a distinct advantage of using BO values to quantitatively assess the bond strength as opposed to simply using the atomic separations, or the alignment of peaks in the atom-resolved partial DOS (PDOS). BO ($\rho_{\alpha\beta}$) is calculated from:

$$\rho_{\alpha\beta} = \sum_{n,occ} \sum_{i,j} C^{*n}_{i\alpha} C^n_{j\beta} S_{i\alpha,j\beta}. \tag{2}$$

For optical properties calculation, we start with the imaginary component of the complex dielectric function $\varepsilon(\hbar\omega) = \varepsilon_1(\hbar\omega) + i\varepsilon_2(\hbar\omega)$ for interband optical transitions in the random phase approximation (RPA) according to:

$$\varepsilon_2(\hbar\omega) = \left(\frac{e^2}{\pi m E \omega}\right) \int d\vec{k} \sum_{n,l} \left|\psi_n\left(\vec{k},\vec{r}\right)|\vec{P}|\psi_l\left(\vec{k},\vec{r}\right)\right|^2 f_l\left(\vec{k}\right) \times \left[1 - f_n\left(\vec{k}\right)\right] \delta\left[E_n\left(\vec{k}\right) - E_l\left(\vec{k}\right) - E\right] \tag{3}$$

where $E = \hbar\omega$ is the photon energy, $f\left(\vec{k}\right)$ is the Fermi distribution function, l labels an occupied state and n an unoccupied state, and $\psi_n\left(\vec{k},\vec{r}\right)$ is the Bloch wave function for the nth band with energy $E_n\left(\vec{k}\right)$ at Brillouin zone point k. The momentum matrix element (MME) $\psi_n\left(\vec{k},\vec{r}\right)|\vec{P}|\psi_l\left(\vec{k},\vec{r}\right)$ is explicitly calculated from the ab initio wave functions. The real part of the dielectric function $\varepsilon_1(\hbar\omega)$ is then obtained from the imaginary part $\varepsilon_2(\hbar\omega)$ using the Kramers–Kronig transformation.

Elastic stiffness constants are critical for assessing how a solid responds under applied strain within the elastic limit. The elastic tensor enables the evaluation of bulk mechanical properties. In the present study, we use the strain–stress analysis approach [47]. In this approach, a small strain of plus or minus 1 % is applied to each independent strain element in the fully relaxed structure. The six stress components (σ_{ij}) are calculated for each strain ε_j applied to the structure. The elastic coefficients C_{ij} are calculated by solving a set of linear equations:

$$\sigma_{ij} = \sum_{ij} C_{ij}\varepsilon_j \tag{4}$$

From the calculated C_{ij} values, one can obtain bulk mechanical properties (bulk modulus K, shear modulus G, Young's modulus E, and Poisson's ratio η) using the well-known Voight–Reuss–Hill scheme under the polycrystalline approximation [48–50]. We have used this approach to study the mechanical properties of many complex metallic and ceramic crystals in recent years [45, 51].

4. Results and discussion

4.1. Band structure and density of states

The calculated band structures for the five stable phases and the C12A7-electride phase using the OLCAO method are presented in Fig. 3(a)–3(f) along with markers indicating the range of energy differences between different band structures. Overall, the band structures are interesting because of the similarities and distinct differences among them. With the exception of C12A7-electride phase, they are all large band gap insulators with direct band gaps

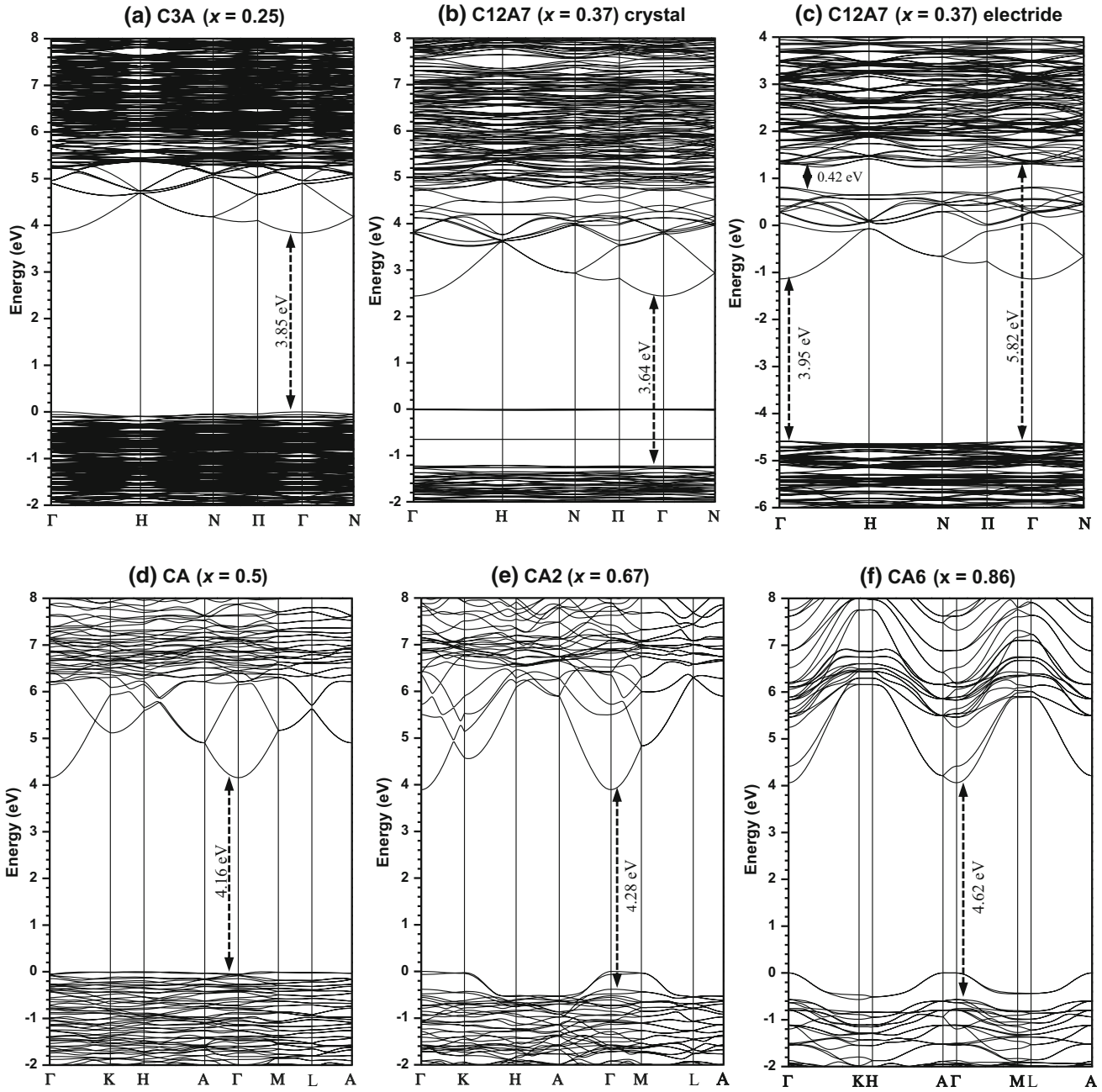

Fig. 3 Calculated band structures of the different calcium aluminate phases

ranging from 3.85 to 4.62 eV at the zone center Γ. The C12A7-electride phase is metallic (The zero of the energy is defined here as the highest occupied level). The top of the bulk VB is flat in four phases while in CA2 and CA6 two extra bands split off from the bulk VB, and for CA6 they separate completely. They originate from the specific O sites (O1 in CA2 and O3 in CA6) which is further discussed later. The variation of the band gap with x in the six calcium aluminate phases (Table 2) shows the trend of increasing band gap (C3A < CA < CA2 < CA6) with increasing alumina content except for the C12A7 phase further discussed below. All calculated band gaps are expected to be smaller than measured values because DFT calculations generally underestimate band gap of insulating materials.

The band structures of C12A7-crystal [Fig. 3(b)] and C12A7-electride phase [Fig. 3(c)] are quite different and deserve special attention. These two crystals are essentially the same in terms of their atomic structure with the distinction that the C12A7-crystal contains O atoms within the

Table 2 Electronic structure, effective charge (Q^*) and bond order (BO) results

	C3A	C12A7-crystal	C12A7-electride	CA	CA2	CA6
x (% of Al_2O_3 content)	0.25	0.37	0.37	0.50	0.67	0.86
Electronic structure						
Band gap (eV)	3.85	3.64	5.82	4.16	4.28	4.62
m^* (electron)	0.42	0.45	NA	0.40	0.41	0.42
m^* (hole)	2.51	22.87	NA	1.77	4.23	3.90
Effective charge (Q^*)						
Ca						
Average Q^*	6.930	6.876, 6.54[a]	6.937	6.817, 6.51[b]	6.814	6.782
Charge transfer (ΔQ^*)	−1.070	−1.124	−1.053	−1.183	−1.186	−1.218
Al						
Average Q^*	1.560	1.516, 1.41[a]	1.547	1.527, 1.42[b]	1.474	1.566
Charge transfer (ΔQ^*)	−1.440	−1.484	−1.453	−1.473	−1.526	−1.434
O						
Average Q^*	7.015	7.038, 7.20[a]	7.034	7.032, 7.16[b]	7.041	6.970
Charge transfer (ΔQ^*)	+1.015	+1.038	+1.034	+1.032	+1.041	+0.970
Bond Order (BO)						
Total BO	76.71	36.30	34.03	18.59	16.75	25.87
Cell Vol. Å^3	3646.11	1758.54	1770.81	719.85	612.08	602.86
TBOD (BO/Vol.)	0.0211	0.0206	0.0193	0.0258	0.0274	0.0429

[15] [a] C12A7-crystal, [b] 50CaO-crystal

cage structures. The variation in band structure between the C12A7-cyrstal and C12A7-electride phases is due primarily to the removal of the O atoms. Now, looking at the C12A7-crystal, there are two occupied defect states near the top of the VB. These states are identified with the two O atoms located inside two of the twelve nano-cages of C12A7-crystal. Without those two O atoms, on the other hand, the C12A7-electride is metallic. The band structure of the C12A7-electride phase does not have any defect states near the main part of the VB and the lower part of the electride CB has detached similar to the structure in C12A7-crystal. The variation in the band structures between the two C12A7 phases are quite distinctive, and we believe that for such cases it is beneficial to introduce names for the different components to clearly discuss their relationship. The upper part (from ~1.23 eV on up) originates from cation sites of the framework (the "framework conduction band", or FCB), whereas the lower and narrower part (from −1.14 eV to 0.81 eV) is formed by the states associated with the cages (the "cage conduction band", or CCB). The highest occupied state, which is at 0.0 eV, is identified as the Fermi level energy, E_F. There is a large gap of 3.95 eV within the occupied region of the band structure between the top of the main part of the VB (at −4.60 eV) and the bottom of the CCB (at −1.14 eV). As observed in the study of the density of states (DOS) below, there is some degree of isolation of electronic states so that it is perhaps more appropriate to define the "gap" of the electride phase to be 5.82 eV going between the main part of the VB and the FCB. In this model there would be metallic bands within this large gap. McLeod et al. [13] have reported this interpretation of the band gap to be 5.9 eV based on experimental measurements (XPS, XES and XAS). Our calculated values are in good agreement with their results. The separation between FCB and CCB of 0.42 eV is quite small. The origin of these metallic bands in C12A7-electride is from the removal of extra-framework species (O3 sites) and the resultant softening of the cage-like structures. We anticipate that future modification of the C12A7 structure (perhaps via variation in O content of via the inclusion of other elements within the cage structures) could in-turn modify the band structure in a controllable way.

The effective masses m^* of charge carriers in crystals are important for their transport properties. Each of the stable phases may be p- or n-doped so as to encourage either hole or electron conduction. Our calculations predict the effective masses of the particle that may be induced to conduct via one form of doping or the other. The electron effective masses m_e^* and hole effective masses m_h^* for the five stable phases and the C12A7-electride phase are listed in Table 2. As can be seen from the band structures, a large anisotropy exists. The electron effective masses are much smaller than the hole effective masses due to the very flat top of the VB. The m_e^* for these crystals are surprisingly close (in a narrow range of 0.40–0.45) electrons and

comparable to those in typical semiconductors whereas the heavy m_h* vary substantially. These effective mass values indicate that it would be preferable to induce electrons to be the charge carriers via doping.

Figure 4 shows the calculated total and partial density of states (DOS) of the six phases of the Ca–Al–O series. The inclusion of partial DOS (PDOS) in the discussion is for the purpose of tracing specific features in the DOS to particular atomic sites in the crystal. We have aligned the zero of the energy to be at the top of the VB for easy comparison whereas in Fig. 3 for band structures, the zero of the energy is defined as the highest occupied state. Thus, the C12A7-electride phase has 0 eV at the top of the main part of the VB, not at E_F. As is typical of most oxide compounds, the upper (lower) VB is from the O-2*p* (O-2*s*) orbitals for each crystal. Further, the large peak between −18 and −20 eV comes from the semi-core Ca 3*p* levels. The usefulness of the PDOS is to allow for comparison of the contributions to the total DOS from crystallographically different Ca, Al, and O sites. For example, in CA phase [Fig. 4(d)], there are two Ca, four Al, and eight O sites but their PDOS are almost the same within each species while in the C3A

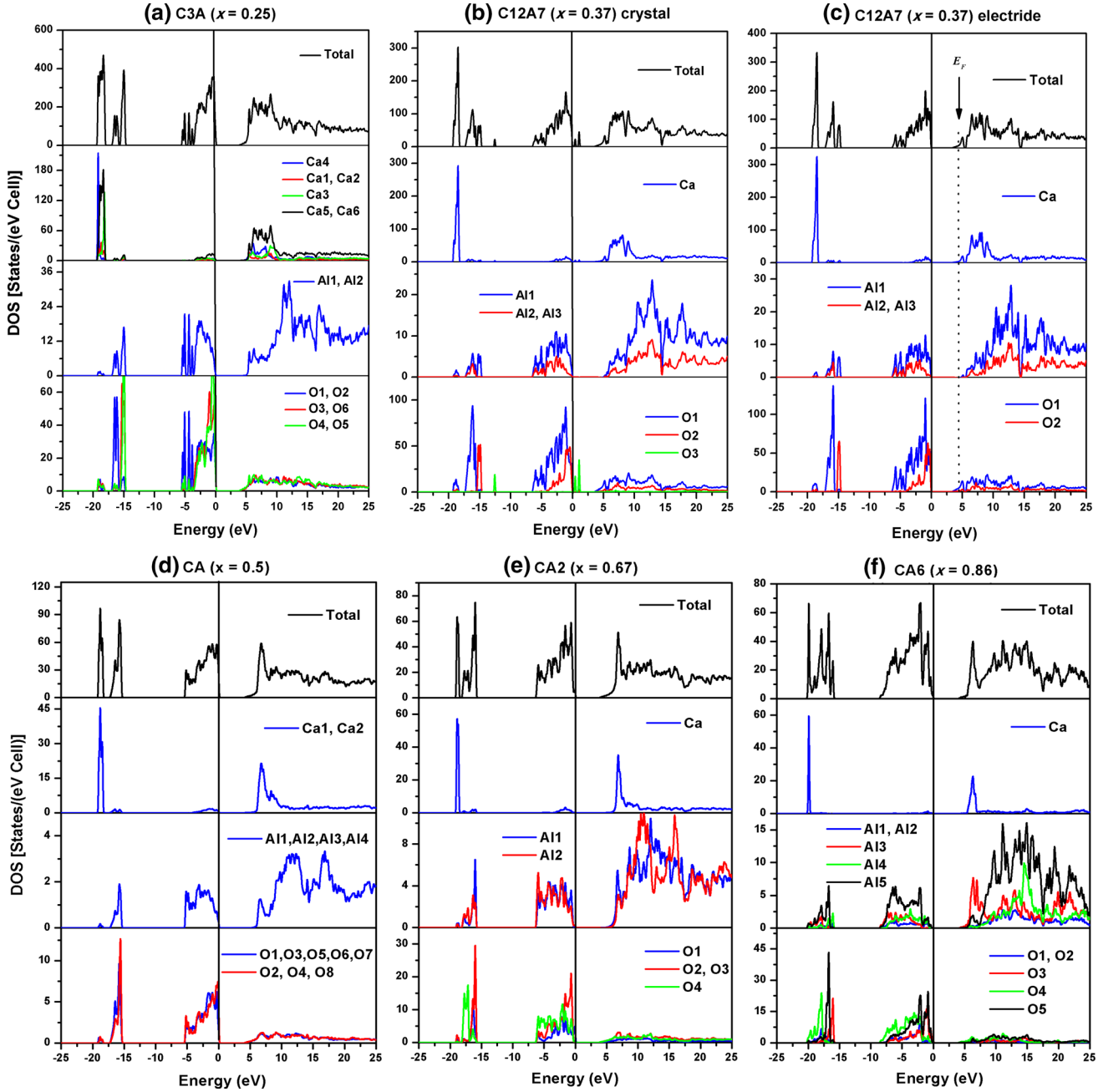

Fig. 4 Calculated total and partial DOS of the different calcium aluminate phases

phase [Fig. 4(a)], there are six Ca sites, two Al sites, and six O sites with varying degrees of difference between them.

Looking at the C12A7-crystal and C12A7-electride phases [Fig. 4(b) and 4(c)] we see that the gross features are approximately the same because the framework structures of the two are the same. However, the first key difference is the presence or absence of O3 which contributes two small peaks in C12A7-crystal and whose absence is then associated with the different band structure of C12A7-electride. Interestingly, via the PDOS, we see that the CCB in the C12A7-electride can be associated most clearly with O1 and Ca and to a much lesser extent with Al1 and O2. Our TDOS for the two C12A7 phases agree well with those reported by Sushko [14] and McLeod et al. [13] with minor differences in peak positions.

The total DOS (TDOS) and PDOS of CA, CA2 and CA6 are shown in Fig. 4(d)–4(f). Like the band structures discussed previously, they are somewhat similar in both the VB and CB regions with the width of the upper VB increasing as the alumina content increases. The remaining variations in the PDOS of the crystals reflect the variations in local bonding and environment. As one example, considering CA6, the PDOS of each Al type is quite different (except for Al1 and Al2). This can be easily rationalized by the following facts: (a) Al1 and Al2 are sixfold [BLs: 1.89 Å (3) and 1.90 Å (3)] and fivefold [BLs: 2.00, 2.48, and 1.77 Å (3)] coordinated respectively, Al3 is fourfold coordinated [BLs: 1.83, 1.80 Å (3)]. Al4 is sixfold coordinated [BLs: 1.98 Å (3) and 1.90 Å (3)] and Al5 is sixfold coordinated (BLs: 1.88, 1.99, 2.01 Å (2), and 1.82 Å (2). Such diversity in local bonding environments explains the difference in their PDOS in Fig. 4. Such differences are further illustrated in the bond order and effective charge calculations later.

4.2. Effective charges and bond order

BO and effective charge Q_α* on atom α are important physical quantities that describe the bonding of atoms and charge transfer effects in solids. They indicate the relative ionicity in these crystals. In Table 2 we list the calculated average Q_α* and total BO values. The Q_α* values for atoms at each nonequivalent site (not tabulated) can differ similar to what is shown in the PDOS in Fig. 4. Akola et al. [15] have calculated the Ca, Al, and O effective charges for C12A7-crystal/64CaO-glass and 50CaO-crystal/50CaO-glass using combined DFT-RMC simulations. Their results are also listed in Table 2 for comparison. The slight difference from our results can be attributed to the difference in the methods of calculation and the underlying structures of the models with our crystals. The charge transfer $\Delta Q^* = Q^* - Q_o$ (Q_o is the valence electron number in the neutral atom) of Ca, Al, and O atoms in the six calcium aluminate phases are also presented in Table 2 (the minus sign indicates a loss of electrons and a positive sign represents a gain of electrons). As expected for any ionic insulator, the cations (Ca and Al) lose charge to the anions (O). Ca atoms are more ionic than Al atoms and the relative ionicity in the series decreases as alumina content increases. The same can be concluded for O atoms. We note that in CA6, the ΔQ^* trend for O is broken due to the significant alumina content which is less ionic than CaO and the highly anisotropic crystal structure for CA6. In the C12A7 systems, the average Q_{Ca}* in C12A7-electride (6.94 electrons) is slightly higher than in the C12A7-crystal phase (6.88 electrons). Extra-framework oxide O^{2-} ions in C12A7-crystal interact strongly with the cage Ca atoms as can be seen from the PDOS [Fig. 4(b)] and are responsible for this difference.

The totality of bond orders which depends on the number of bonds and the strength of each bond pair is a compelling indicator of the overall crystal cohesion. Figure 5 shows the distribution of the calculated BO values of different types of bonds (Al–O and Ca–O) in the five stable calcium aluminates. We have not included the results for C12A7-electride because it has the same bonding environment as that of C12A7-crystal. The calculated total BO (TBO) and the total bond order density (TBO per unit volume, TBOD) are also listed in Table 2. The concept of TBOD is a very useful one because it is a single parameter signifying the cohesion of a crystal.

The BO values scale with BL as can be seen from Fig. 5. The stronger BOs are from Al–O bonds (open symbols) (BL $<$ 2.03 Å) and the weaker BOs are from Ca–O bonds

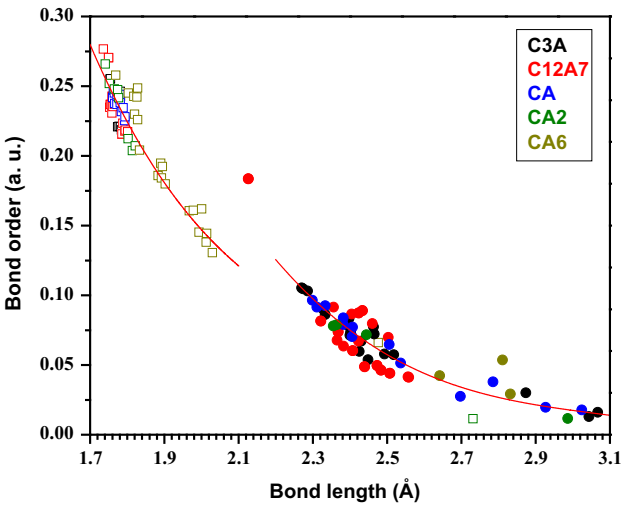

Fig. 5 (*Color online*) Distribution of bond order versus bond length for all stable phases of the calcium aluminate system. The *open symbols* represent Al–O type bonds and *filled symbols* represent Ca–O bonds

Table 3 Calculated and measured bulk mechanical properties of calcium aluminates

Crystal	x	Elastic moduli tensor coefficients									Bulk mechanical properties			
		C_{11}	C_{22}	C_{33}	C_{44}	C_{55}	C_{66}	C_{12}	C_{13}	C_{23}	K (GPa)	G (GPa)	E (GPa)	η
C3A	0.25	163.7			52.8			68.9			100.5	50.5	129.8	0.28
		169.8[9]			53.7[9]			68.3[9]			102.1[9]	52.5[9]	134.4[9]	0.28[9]
		172.1[7]			56.1[7]			68.3[7]			102.9[7]	54.4[7]	138.7[7]	0.28[7]
													145[8]	
C12A7-crystal	0.37	168.4			48.3			61.0			96.8	50.4	128.8	0.28
		170.0[53]			52[53]			56[53]						
C12A7-electride	0.37	157.2			48.9			64.6			95.5	47.8	122.9	0.28
CA	0.50	88.9	155.8	183.1	40.2	50.0	41.2	33.0	58.3	55.0	75.0	43.2	108.8	0.26
CA2	0.67	172.0	198.5	199.2	57.7	41.7	32.4	74.3	80.3	73.2	113.2	45.8	120.9	0.32
CA6	0.86	371.8		254.1	93.2		99.3	172.6	92.2		183.7	99.0	251.7	0.27
													$294_{\parallel}$[54], $309_{\perp}$[54]	

(solid symbols) (BL > 2.28 Å). CA6 has 97 % of its total BO values from interlayer and intra-layer Al–O bonds and only 3 % from interlayer Ca–O bonds. Thus, the Al–O bonds are the dominant contributor and the overall stiffness and anisotropy must be related to the aluminate chain orientation in calcium aluminate crystals. In CA6, Al–O (Al2-O1) bonds that are parallel to the *c*-axis (with BL of 2.48 Å) are much weaker and have very low BO (0.0661) values. They contribute very little to the total Al–O BO. Similar trends can be easily traced out for the other phases. There are a few weaker Al–O bonds with much larger BLs. For example, in the CA2 phase, co-planar Al–O (Al2–O1) bonds are much weaker, with BO/BL values of 0.01/2.73 Å. The weaker Ca–O bonds in these crystals shown in Fig. 5 cover a much wide range of BL distributions from 2.27 Å onward. As a whole, both bond types (Al–O and Ca–O) can be described as prominently ionic but we observe that the Al–O bonds are shorter with more covalent character.

To make our results more meaningful, we have also provided the TBOD for different values of x in Table 2. As can be seen, CA6 has the largest TBOD and C12A7-crystal the smallest among the five stable calcium aluminate phases. These TBOD results are consistent with the fact that CA6 is the hardest (having the highest melting point) and C12A7-crystal is the softest (having the lowest melting point) among the stable calcium aluminates. As for the two phases of C12A7, the electride phase has a slightly smaller TBOD value than the crystal phase. This is expected because the removal of extra-framework O ions results in the weakening of the cage-like structure.

4.3. Mechanical properties

Our calculated elastic stiffness constants for the five stable calcium aluminates and one C12A7-electride phase

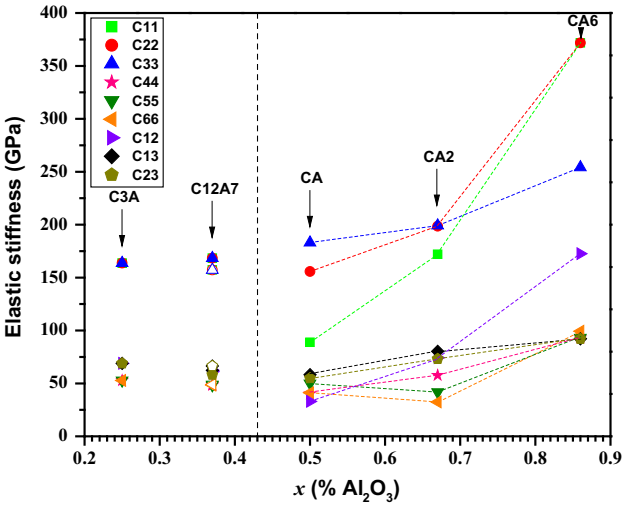

Fig. 6 (*Color online*) Calculated elastic constants of the studied calcium aluminate phases in GPa. *Open symbols* represent the C12A7-electride

are listed in Table 3 and also plotted in Fig. 6 for visual analysis of trends and easy comparison among different phases. To our knowledge, this is the only complete analysis of the mechanical properties of the Ca–Al–O series. There are substantial diversities in the elastic behavior amongst the calcium aluminates. Due to their cubic symmetry, the C3A and C12A7 phases have only three independent tensor elements: C_{11}, C_{44}, and C_{12}. CA and CA2 are monoclinic crystals, so they have nine elastic coefficients: C_{11}, C_{22}, C_{33}, C_{44}, C_{55}, C_{66}, C_{12}, C_{13}, and C_{23}. The hexagonal CA6 has six independent tensor coefficients: C_{11}, C_{33}, C_{44}, C_{66}, C_{12}, and C_{13}. Figure 6 shows that the elastic behavior of the calcium aluminates can be roughly divided into two categories. The first category is composed of the cubic phases C3A and C12A7 (both crystal and electride). They are relatively weaker because of the

abundance of Ca–O bonds, which are less strong than the Al–O bonds. The elastic constant C_{11} is much larger than C_{44} and C_{12} indicating that these crystals are stronger along the three crystallographic axes. The structures are also more closely packed in the axial direction. For the C3A phase, we have also included results from previous calculations and measurements [7–9] in Table 3. Our results for the elastic coefficients C_{44} and C_{12} are in very good agreement with those of Ref. [7, 9]. The difference for C_{11} is no more than 3.7 % from [9] and 5.1 % from [7]. For C12A7-crystal, our results are also in very good agreement with the experimental results reported by Whatmore [52]. The maximum differences for C_{11}, C_{12} and C_{44} are no more than 0.95, 8.2, and 7.7 % respectively.

In the second category (CA, CA2, and CA6) with higher Al_2O_3 content we see highly anisotropic behavior of the phases. CA has smaller C_{11} and C_{22} compared to C_{33}, reflecting that the structure is relatively open and loosely packed along the crystallographic a and b-axes. Al_2O_3 chains align along the c-axis, making it stiffer, resulting in larger values of C_{33}. CA2 has a very long a-axis. The crystal structure is loosely packed along this direction resulting in smaller C_{11}. The b and c-axes are relatively shorter and more closely packed with Al_2O_3 chains, resulting in higher values for C_{22} and C_{33}. The off-diagonal coefficients (C_{12}, C_{13}, and C_{23}) appear to be larger than the shear stiffness constants (C_{44}, C_{55}, and C_{66}) in this crystal. On the other hand, the elastic behavior of the hexagonal CA6 is far more anisotropic with C_{11} and C_{22} and is larger than C_{33}. Thus, CA6 is weak along the c-axis resulting in smaller C_{33}. We have already alluded in last section to the notion that some of the Al–O bonds along the c-axis are very weak (as shown in Fig. 5), while the Al–O bonds along a and b axes are very strong. CA6 has the highest values for all of the elastic constants and is the hardest phase among the calcium aluminate oxides as discussed in the previous section on BO calculations. We are not aware of any measured or calculated data on the elastic stiffness constants of CA, CA2 and CA6 to compare with our calculated values.

From the calculated elastic stiffness coefficients, we have obtained the bulk mechanical properties: bulk modulus (K), shear modulus (G), Young's modulus (E) and Poisson's ratio (η) using the well-known VRH approximation [48–50]. These are listed in Table 3 together with a few calculated/measured values from the literature. We have displayed the calculated values of K, G, E, and η as a function of x in Fig. 7. Their trends mimic that of the elastic coefficients of Fig. 6 in the two roughly divided categories. K generally increases with x excluding the CA phase. G increases from $x = 0.25$ to $x = 0.37$, decreases at $x = 0.5$ and then keeps on increasing up to $x = 0.86$. Young's modulus E follows the same pattern as the shear

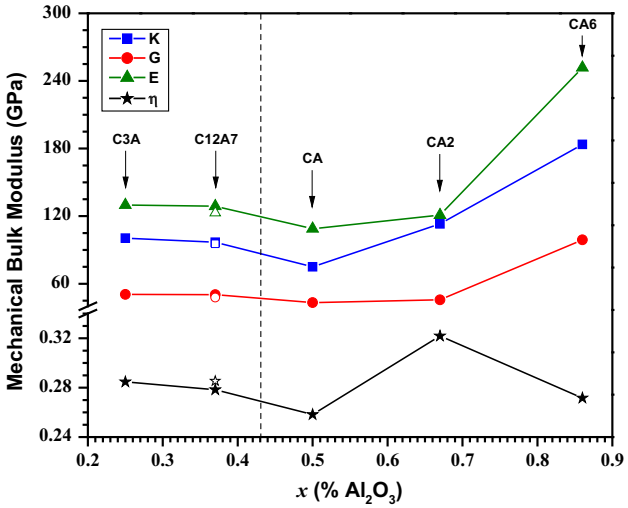

Fig. 7 (*Color online*) Calculated bulk mechanical properties of the studied calcium aluminate phases. *Open symbols* represent the C12A7-electride

modulus. The variation in Poisson's ratio η tends to be more irregular with no clear trend with x. The calculated mechanical parameters (K, G, and E) for the C12A7-electride phase has values that are slightly lower than those of C12A7-crystal because removing the extra-framework O ions makes the C12A7-electride structure slightly weaker. A comparison of our calculated bulk mechanical properties with reported values (calculated and measured) is presented in Table 3. In C3A, there are large variations among Young's modulus, presumably due to different methods used in the calculations [7, 9] or measurement with nanoindentation experiments [8]. Nagaoka [53] measured the elastic moduli of CA6 ceramics prepared by a hot-pressing technique. The measured values of elastic moduli along surfaces parallel and perpendicular to the hot-pressing direction (labeled as $\parallel$ and $\perp$) has a difference of 15 GPa. Our calculated values are somewhat smaller. These differences arise from high pressure/temperature exerted during the formation/measurement of the CA6 ceramic samples. We are not able to find any data for the rest of the Ca–Al–O phases and our results now stand as predicted values for ideal crystalline phases waiting for future verification.

4.4. Optical properties

The interband optical properties of the studied phases of calcium aluminate are computed in the form of frequency-dependent complex dielectric functions $\varepsilon(\omega) = \varepsilon_1(\omega) + i\varepsilon_2(\omega)$. The $\varepsilon_2(\omega)$ spectra are obtained first from Eq. (3) and then $\varepsilon_1(\omega)$ is obtained from $\varepsilon_2(\omega)$ via Kramers–Kronig-conversion. The calculation includes the momentum matrix elements from the occupied VB states to the empty CB

states. Figure 8(a)–8(f) shows the calculated $\varepsilon_1(\omega)$ and $\varepsilon_2(\omega)$ curves for frequencies up to 35 eV. From the zero frequency limit of the real part of the dielectric function $\varepsilon_1(0)$ (the static optical dielectric constant), the refractive indices of the various phases of calcium aluminates can be estimated using a simple relation: $n = \sqrt{\varepsilon_1(0)}$. In Table 4 we summarize these results on optical properties along with various data reported in the literature [37, 54–57]. Both the calculations and the results from previous literature reveal that C3A has the highest refractive index (1.85/1.71) and C12A7 has the lowest value (1.66/1.64). Although the calculated values are larger than those reported especially for C3A, we observe that the calculated refractive index as a function of x varies in a zig-zag fashion consistent with the previously reported data.

From the spectra we note that each structure has its own set of unique peak features (labeled as A–D with some primed labels). The spectral features of C12A7-electride [Fig. 8(c)] are very different from the other crystal phases in the low frequency region from 0 to 5 eV because it has metallic bands with a Fermi surface. Thus, the $\varepsilon_2(\omega)$ curve at zero frequency extends to infinity. It is our intention that these predictive results find used in ongoing experimental efforts to characterize crystalline, polycrystalline, or amorphous samples in the Ca–Al–O series, especially for the two C12A7 phases.

5. Conclusions

We have presented a comprehensive investigation of the electronic structure, bonding, mechanical, and optical properties of the five stable phases in calcium aluminate series and the C12A7-electride phase with comparative studies. The comprehensive nature of the investigation covering all known phases and their physical properties provide an overview picture for this important class of ceramic materials. The results can be succinctly summarized as follows. Although the calcium aluminates contain the same chemical species, Ca, Al, and O, the coordination and local environments of these species are very different resulting in very different structural and physical properties depending on the CaO/Al_2O_3 ratio and crystal structures. Electronic structure calculations show that all stable phases of calcium aluminates are large band gap insulators with the C12A7-electride being the most fascinating. It contains metallic bands associated with atoms defining the cage structure which are generally distinct from those defining the framework. The presence of partially occupied cages by O atoms in the cages of the network structure in C12A7-crystals and C12A7-electride resulted in many unusual properties that can be explored for potential applications. In a strict sense, C12A7 is more appropriate to be classified as a defective crystal with no long range order. Through effective charge and bond order calculations, quantitative information on the nature of Ca–O and Al–O bonding and ionic charge transfer in relation to the alumina content is

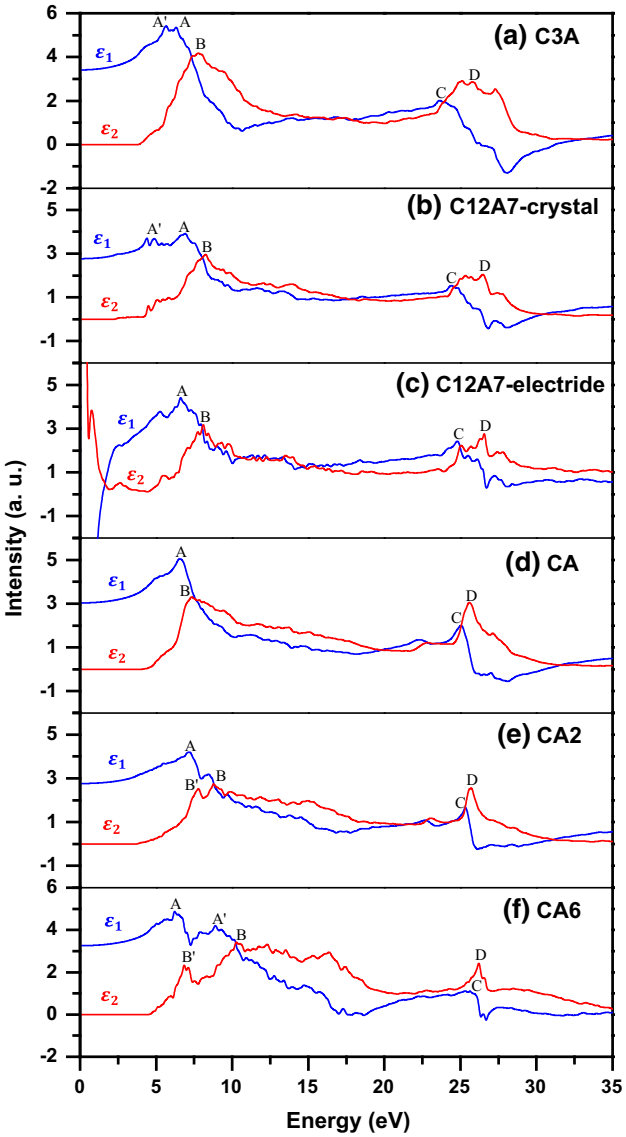

Fig. 8 (*Color online*) Calculated real and imaginary parts of the dielectric functions of five stable and one C12A7-electride calcium aluminate oxide phase

Table 4 Optical properties

Crystal	x	ε_1 (0)	$n = \sqrt{\varepsilon_1(0)}$
C3A	0.25	3.417	1.85 (1.71[55])
C12A7	0.37	2.766	1.66 (1.64[56])
CA	0.50	3.034	1.74 (1.67[57])
CA2	0.67	2.759	1.66 (1.65[37])
CA6	0.86	3.253	1.80 (1.70[58])

revealed. We contend that the total bond order density (TBOD) is a single most useful parameter for the quantitative evaluation of the cohesion in these crystals. CA6 crystal, with its largest TBOD, is the most suitable candidate for use in high-temperature environments. The elastic and mechanical properties show a high degree of diversity and anisotropic behavior that can be related to the fundamental electronic structure through bond order values depending on their complex crystal structures. The optical properties calculations provide the refractive index data and their variations with alumina content. The highest refractive index (1.85) is from C3A and the lowest value (1.66) is from C12A7, consistent with measured data.

Acknowledgments This work was supported by U.S. DOE Grant No. DE-FG02-84DR45170 and later in part by NSF Grant CMMI-1068528. This research used the resources of NERSC supported by the Office of Science of DOE under the contract No. DE-AC03-76SF00098.

References

1. Y Wang and S Diamond *Mater. Res. Soc. Symp. Proc.* **370** 23 (1995)
2. D Sohn and T O Mason *J. Adv. Cem. Based Mater.* **7** 81 (1998)
3. L M Schwartz, E J Garboczi and D P Bentz *J. Appl. Phys.* **78** 5898 (1995)
4. H F W Taylor *Cement Chemistry*, 2nd edn. (UK: Thomas Telford) vol 19 (1990)
5. H C Yi, J Y Guigne, J J Moore, F D Schowengerdt, L A Robinson and A R Manerbino *J. Mater. Sci.* **37** 4537 (2002)
6. J E Medvedeva, E N Teasley and M D Hoffman *Phys. Rev. B Condens. Matter Mater. Phys.* **76** 155107 (2007)
7. H Manzano, J S Dolado and A Ayuela *J. Am. Ceram. Soc.* **92** 897 (2009)
8. K Velez, S Maximilien, D Damidot, G Fantozzi and F Sorrentino *Cem. Concr. Res.* **31** 555 (2001)
9. J Moon, S Yoon, R M Wentzcovitch, S M Clark and P J M Monteiro *J. Am. Ceram. Soc.* **95** 2972 (2012)
10. K Hayashi, S Matsuishi, T Kamiya, M Hirano and H Hosono *Nature* **419** 462 (2002)
11. M Ruszak, M Inger, S Witkowski, M Wilk, A Kotarba and Z Sojka *Catal. Lett.* **126** 72 (2008)
12. S W Kim et al. *Nano Lett.* **7** 1138 (2007)
13. J A McLeod et al. *Phys. Rev. B Condens. Matter Mater. Phys.* **85** 045204 (2012)
14. P V Sushko, A L Shluger, Y Toda, M Hirano and H Hosono *Proc. R. Soc. A* **1** 1 (2011)
15. J Akola et al. *PNAS Early Edition* **1** 1 (2013)
16. S W Kim, T Shimoyama and H Hosono *Science* **333** 71 (2011)
17. S Jonas, F Nadachowski and D Szwagierczak *Ceram. Int.* **25** 77 (1999)
18. M K Cinibulk and R S Hay *J. Am. Ceram. Soc.* **79** 1233 (1996)
19. W Y Ching and P Rulis *Electronic Structure Methods for Complex Materials: The Orthogonalized Linear Combination of Atomic Orbitals* (UK: Oxford University Press) vol 1 (2012)
20. G Kresse and J Hafner *Phys. Rev. B Condens. Matter Mater. Phys.* **47** 558 (1993)
21. G Kresse and J Furthmüller *Comput. Mater. Sci.* **6** 15 (1996)
22. A Hussain, S Aryal, P Rulis, M A Choudhry, J Chen and W Y Ching *J. Alloys Compd.* **509** 5230 (2011)
23. C C Dharmawardhana, A Misra, S Aryal, P Rulis and W Y Ching *Cem. Concr. Res.* **52** 123 (2013)
24. W Y Ching, Y Mo, S Aryal and P Rulis *J. Am. Ceram. Soc.* **96** 2292 (2013)
25. N Li, R Sakidja, S Aryal and W Y Ching *Phys. Chem. Chem. Phys.* **16** 1500 (2014)
26. V L Burdick and D E Day *J. Am. Ceram. Soc.* **50** 97 (1967)
27. P Mondal and W Jeffery *Acta Crystallogr.* **31** 689 (1975)
28. M Collepardi, G Baldini and M Pauri *Cem. Concr. Res.* **8** 571 (1978)
29. H Bartl and T Scheller *Mineral. Monatsh.* **35** 547 (1970)
30. H Boysen, M Lerch, A Stys and A Senyshym *Acta Crystallogr.* **B63** 675 (2007)
31. W Horkner and H K Muller-Buschbaum *J. Inorg. Nuclear Chem.* **38** 983 (1976)
32. B Tavisci *Tonindustrie-Zeitung* **61** 717 (1937)
33. V K Lagerqvist, S Wallmark and A Westgren *Zeitschrift Für Anorganische und Allgemeine Chemie* **234** 1 (1937)
34. J R Goldsmith *J. Geol.* **56** 80 (1948)
35. C Goria and A Burdese *La Ricerca Scientifica* **21** 1613 (1951)
36. N E Filonenko and I V Lavrov *J. Appl. Chem. (USSR)* **23** 1040 (1950)
37. E R Boyko and L G Wisnyi *Acta Crystallogr.* **11** 444 (1958)
38. B Cockayne and D S Robertson *Solid State Commun.* **2** 359 (1964)
39. D W Goodwin and A J Lindop *Acta Crystallogr.* **B26** 1230 (1970)
40. A Utsunomiya, K Tanaka, H Morikawa, F Marumo and H Kojima *J. Solid State Chem.* **75** 197 (1988)
41. P Hohenberg and W Kohn *Phys. Rev.* **136** B864 (1964)
42. W Kohn and L J Sham *Phys. Rev.* **140** A1133 (1965)
43. A Hussain, S Aryal, P Rulis, M A Choudhry and W Y Ching *Phys. Rev. B Condens. Matter Mater. Phys.* **78** 195102 (2008)
44. Y Mo, P Rulis and W Y Ching *Phys. Rev. B* **86** 165122 (2012)
45. W Y Ching, P Rulis, L Ouyang, S Aryal and A Misra *Phys. Rev. B* **81** 214120 (2010)
46. R S Mulliken *J. Chem. Phys.* **23** 1841 (1955)
47. H Yao, L Ouyang and W Y Ching *J. Am. Ceram. Soc.* **90** 3194 (2007)
48. W Voigt *Lehrbuch der Kristallphysik* (Germany: L Berlin and B G Teubner) (1928)
49. A Reuss *Z. Angew. Math. Mech.* **9** 49 (1929)
50. R Hill *Proc. Phys. Soc. A* **65** 349 (1952)
51. C C Dharmawardhana, R Sakidja, S Aryal and W Y Ching *APL Materials* **1** 012106 (2013)
52. R W Whatmore, C O Hara, B Cockayne and G R Jones *Mater. Res. Bull.* **14** 967 (1979)
53. T Nagaoka, S Kanzaki and Y. Yamaoka *J. Mater. Sci. Lett.* **9** 219 (1990)
54. *Sample dispersion and refractive index guide* Man 0079 *Version 3.1* (United Kingdom: Malvern Instruments Ltd.) 1.24 (1997)
55. http://en.wikipedia.org/wiki/Mayenite
56. L G Hwa, C C Chen and S. L. Hwang *Chin. J. Phys.* **35** 78 (1997)
57. G N Mohanty *Ph.D. Thesis* (University of Missouri, USA) (1954)